Inorg. Chem. **2008**, *47*, 9459−9470

Large Mn_{25} Single-Molecule Magnet with Spin $S = {}^{51}/_{2}$: Magnetic and High-Frequency Electron Paramagnetic Resonance Spectroscopic Characterization of a Giant Spin State

Muralee Murugesu,[†] Susumu Takahashi,[‡] Anthony Wilson,[‡] Khalil A. Abboud,[†] Wolfgang Wernsdorfer,[§] Stephen Hill,[‡] and George Christou*[,†]

Department of Chemistry, University of Florida, Gainesville, Florida 32611-7200, Department of Physics, University of Florida, P.O. Box 118440, Gainesville, Florida 32611, and Institut Néel, CNRS, BP 166, 25 Avenue des Martyrs, 38042 Grenoble, Cedex 9, France

Received June 20, 2008

The synthesis and structural, spectroscopic, and magnetic characterization of a Mn_{25} coordination cluster with a large ground-state spin of $S = {}^{51}/_{2}$ are reported. Reaction of $MnCl_2$ with pyridine-2,6-dimethanol ($pdmH_2$) and NaN_3 in MeCN/MeOH gives the mixed valence cluster $[Mn_{25}O_{18}(OH)_2(N_3)_{12}(pdm)_6(pdmH)_6]Cl_2$ (**1**; $6Mn^{II}$, $18Mn^{III}$, Mn^{IV}), which has a barrel-like cage structure. Variable temperature direct current (dc) magnetic susceptibility data were collected in the 1.8−300 K temperature range in a 0.1 T field. Variable-temperature and -field magnetization (M) data were collected in the 1.8−4.0 K and 0.1−7 T ranges and fit by matrix diagonalization assuming only the ground state is occupied at these temperatures. The fit parameters were $S = 51/2$, $D = -0.020(2)$ cm^{-1}, and $g = 1.87(3)$, where D is the axial zero-field splitting parameter. Alternating current (ac) susceptibility measurements in the 1.8−8.0 K range and a 3.5 G ac field oscillating at frequencies in the 50−1500 Hz range revealed a frequency-dependent out-of-phase (χ_M'') signal below 3 K, suggesting **1** to be a single-molecule magnet (SMM). This was confirmed by magnetization vs dc field sweeps, which exhibited hysteresis loops but with no clear steps characteristic of resonant quantum tunneling of magnetization (QTM). However, magnetization decay data below 1 K were collected and used to construct an Arrhenius plot, and the fit of the thermally activated region above ∼0.5 K gave $U_{eff}/k = 12$ K, where U_{eff} is the effective relaxation barrier. The g value and the magnitude and sign of the D value were independently confirmed by detailed high-frequency electron paramagnetic resonance (HFEPR) spectroscopy on polycrystalline samples. The combined studies confirm both the high ground-state spin $S = {}^{51}/_{2}$ of complex **1** and that it is a SMM that, in addition, exhibits QTM.

Introduction

Molecular materials that in their ground state possess a large number of unpaired electrons (i.e., a large value of the spin quantum number, S) represent a fascinating research area for a variety of reasons, not least of which is the fact that they are exceptions to the rule that unpaired electrons will normally find ways of pairing up if they can. Although they are in the minority among molecular compounds, such species with large S values are nevertheless a family of great importance to diverse areas of chemistry, physics, materials science, and medicine. Their synthesis and study are thus stimulated by many factors. At one extreme, there is the purely fundamental desire to understand exactly how the large S value arises, that is, how the sign and relative magnitudes of the constituent exchange interactions between the constituent spin carriers (almost always metal ions) leads to a high overall S value. At the other extreme are various potential or actual applications that take advantage of the resulting magnetic properties; examples include relaxation agents for use in, for example, medical MRI techniques,[1] and a molecular ("bottom-up") approach to nanoscale mag-

* To whom correspondence should be addressed. E-mail: christou@chem.ufl.edu.
[†] Department of Chemistry, University of Florida.
[‡] Department of Physics, University of Florida.
[§] Institut Néel, CNRS/UJF.

(1) Rodriguez, E.; Roig, A.; Molins, E.; Arus, C.; Quintero, M. R.; Cabanas, M. E.; Cerdan, S.; Lopez-Larrubia, P.; Sanfeliu, C. *NMR Biomed.* **2005**, *18*, 300.

10.1021/ic801142p CCC: $40.75
Published on Web 09/13/2008

netism.[2] The latter are the single-molecule magnets (SMMs), which are individual molecules that function as nanoscale magnets.[2] For such reasons, we have a longstanding interest in (i) synthesizing and studying new species with large S values;[3] (ii) reaching an understanding of the various factors that lead to their large S value, quantitatively, if possible, by determining the various exchange parameters, or at least qualitatively from the structural parameters;[4] and (iii) using this knowledge to accomplish targeted changes to the S value of a given molecule as a preliminary step in developing some rudimentary level of control of S in such often high-nuclearity molecules.[5]

There are now a significant number of high-spin molecules, most of them in Mn chemistry, and they encompass S values up to $S = {}^{83}/_{2}$ in a Mn_{19} complex.[3−7] In a general sense, large S values can arise from ferromagnetic interactions and/or competing antiferromagnetic interactions (spin frustration) in certain M_x (M = metal) topologies that prevent (frustrate) the preferred antiparallel spin alignments, often leading to intermediate spin alignments.[8] Such spin frustration effects are almost always present in high nuclearity metal clusters because they almost always contain triangular M_3 subunits, and the vast majority of exchange interactions are antiferromagnetic. Thus, this complexity typically prevents ready rationalization of the S value.

Our own work in Mn chemistry has been primarily directed at the synthesis and study of SMMs, species that derive their properties from the combination of a large S and a negative zero-field splitting (ZFS) parameter, D, and thus have a significant barrier to magnetization relaxation.[2,4,9] Within the SMM field, the $[Mn_{12}O_{12}(O_2CMe)_{16}(H_2O)_4]^{z-}$ ($z = 0-3$) family has been the best studied,[2,10] and in our quest for new SMMs, we have explored various synthetic strategies, often involving alkoxide-based chelates.[3−5,11] Of relevance to the present work is the use of pyridine-2,6-dimethanol ($pdmH_2$), which we had found earlier to give Mn products such as Mn_4[12] and Mn_8[13] complexes, depending on the precise reaction conditions. In the additional presence of azide ions, the product was instead a Mn_{25} complex that was found to have a particularly large spin of $S = {}^{51}/_{2}$, the joint highest at that time.[14] This product was also identified as a new SMM, albeit via the combination of its large S value with a clearly very small D value, and we have since carried out a detailed magnetic and Electron Paramagnetic Resonance (EPR) spectroscopic analysis to characterize such parameters in more detail. We also deemed such a study an important foundation that would assist the subsequent extension of the work to structurally perturbed Mn_{25} complexes that undergo a change in ground-state S value, a process we have named "spin tweaking".[4d] We herein describe the results of this study of the properties of a Mn_{25} complex with an $S = {}^{51}/_{2}$ ground state.

(2) For reviews, see:(a) Christou, G.; Gatteschi, D.; Hendrickson, D. N.; Sessoli, R. *MRS Bull.* **2000**, *25*, 66. (b) Aromi, G.; Brechin, E. K. *Struct. Bonding (Berlin)* **2006**, *122*, 1. (c) Christou, G. *Polyhedron* **2005**, *24*, 2065.

(3) (a) Stamatatos, Th. C.; Abboud, K. A.; Wernsdorfer, W.; Christou, G. *Angew. Chem., Int. Ed.* **2006**, *45*, 4134. (b) Stamatatos, Th. C.; Abboud, K. A.; Wernsdorfer, W.; Christou, G. *Polyhedron* **2007**, *26*, 2042. (c) Stamatatos, Th. C.; Poole, K. M.; Abboud, K. A.; Wernsdorfer, W.; OʼBrien, T. A.; Christou, G. *Inorg. Chem.* **2008**, *47*, 5006. (d) Stamatatos, Th. C.; Abboud, K. A.; Wernsdorfer, W.; Christou, G. *Angew. Chem., Int. Ed.* **2008**, *47*, 6694. (e) Tasiopoulos, A. J.; Wernsdorfer, W.; Moulton, B.; Zaworotko, M. J.; Christou, G. *J. Am. Chem. Soc.* **2003**, *125*, 15274. (f) Brechin, E. K.; Sanudo, E. C.; Wernsdorfer, W.; Boskovic, C.; Yoo, J.; Hendrickson, D. N.; Yamaguchi, A.; Ishimoto, H.; Concolino, T. E.; Rheingold, A. L.; Christou, G. *Inorg. Chem.* **2005**, *44*, 502. (g) Moushi, E. E.; Stamatatos, Th. C.; Wernsdorfer, W.; Nastopoulos, V.; Christou, G.; Tasiopoulos, A. J. *Angew. Chem., Int. Ed.* **2006**, *45*, 7722.

(4) (a) Stamatatos, Th. C.; Foguet-Albiol, D.; Stoumpos, C. C.; Raptopoulou, C. P.; Terzis, A.; Wernsdorfer, W.; Perlepes, S. P.; Christou, G. *J. Am. Chem. Soc.* **2005**, *127*, 15380. (b) Stamatatos, Th. C.; Foguet-Albiol, D.; Lee, S.-C.; Stoumpos, C. C.; Raptopoulou, C. P.; Terzis, A.; Wernsdorfer, W.; Hill, S.; Perlepes, S. P.; Christou, G. *J. Am. Chem. Soc.* **2007**, *129*, 9484. (c) Milios, C. J.; Inglis, R.; Vinslava, A.; Bagai, R.; Wernsdorfer, W.; Parsons, S.; Perlepes, S. P.; Christou, G.; Brechin, E. K. *J. Am. Chem. Soc.* **2007**, *129*, 12505. (d) Stamatatos, Th. C.; Abboud, K. A.; Wernsdorfer, W.; Christou, G. *Angew. Chem., Int. Ed.* **2007**, *46*, 884.

(5) Stamatatos, Th. C.; Poole, K. M.; Foguet-Albiol, D.; Abboud, K. A.; O'Brien, T. A.; Christou, G. *Inorg. Chem.* **2008**, *47*, 6593.

(6) Wang, W.-G.; Zhou, A.-J.; Zhang, W.-X.; Tong, M.-L.; Chen, X.-M.; Nakano, M.; Beedle, C. C.; Hendrickson, D. N. *J. Am. Chem. Soc.* **2007**, *129*, 1014. (b) Ge, C.-H.; Ni, Z.-H.; Liu, C.-M.; Cui, A.-L.; Zhang, D.-Q.; Kou, H.-Z. *Inorg. Chem. Commun.* **2008**, *11*, 675.

(7) (a) Ako, A. M.; Hewitt, I. J.; Mereacre, V.; Clérac, R.; Wernsdorfer, W.; Anson, C. E.; Powell, A. K. *Angew. Chem., Int. Ed.* **2006**, *45*, 4926. (b) Ge, C.-H.; Ni, Z.-H.; Liu, C.-M.; Cui, A.-L.; Zhang, D.-Q.; Kou, H.-Z. *Inorg. Chem. Commun.* **2008**, *11*, 675.

(8) (a) Kahn, O. *Molecular Magnetism*; VCH Publishers: New York, 1993. (b) Stamatatos, Th. C.; Christou, G. *Phil. Trans. R. Soc. A* **2008**, *366*, 113; and references therein.

(9) (a) Bircher, R.; Chaboussant, G.; Dobe, D.; Güdel, H. U.; Oshsenbein, S. T.; Sieber, A.; Waldmann, O. *Adv. Funct. Mater.* **2006**, *16*, 209. (b) Gatteschi, D.; Sessoli, R. *Angew. Chem., Int. Ed.* **2003**, *42*, 268. (c) Aubin, S. M. J.; Gilley, N. R.; Pardi, L.; Krzystek, J.; Wemple, M. W.; Brunel, L.-C.; Maple, M. B.; Christou, G.; Hendrickson, D. N. *J. Am. Chem. Soc.* **1998**, *120*, 4991. (d) Oshio, H.; Nakano, M. *Chem.—Eur. J.* **2005**, *11*, 5178. (e) Sessoli, R.; Gatteschi, D.; Caneschi, A.; Novak, M. A. *Nature* **1993**, *365*, 141.

(10) (a) Lis., T. *Acta Crystallogr.* **1980**, *B36*, 2042. (b) Artus, P.; Boskovic, C.; Yoo, Y.; Streib, W. E.; Brunel, L.-C.; Hendrickson, D. N.; Christou, G. *Inorg. Chem.* **2001**, *40*, 4199. (c) Ruiz, D.; Sun, Z.; Albela, B.; Folting, K.; Ribas, J.; Christou, G.; Hendrickson, D. N. *Angew. Chem., Int. Ed. Engl.* **1998**, *37*, 300. (d) Aubin, S. M. J.; Sun, Z.; Guzei, I. A.; Rheingold, A. L.; Christou, G.; Hendrickson, D. N. *J. Chem. Soc., Chem. Commun.* **1997**, 2239. (e) Boskovic, C.; Pink, M.; Huffman, J. C.; Hendrickson, D. N.; Christou, G. *J. Am. Chem. Soc.* **2001**, *123*, 9914. (f) Soler, M.; Artus, P.; Folting, K.; Huffman, J. C.; Hendrickson, D. N.; Christou, G. *Inorg. Chem.* **2001**, *40*, 4902. (g) Chakov, N. E.; Abboud, K. A.; Zakharov, L. N.; Rheingold, A. L.; Hendrickson, D. N.; Christou, G. *Polyhedron* **2003**, *22*, 1759. (h) Chakov, N. E.; Lawrence, J.; Harter, A. G.; Hill, S. O.; Dalal, N. S.; Wernsdorfer, W.; Abboud, K. A.; Christou, G. *J. Am. Chem. Soc.* **2006**, *128*, 6975. (i) Bagai, R.; Christou, G. *Inorg. Chem.* **2007**, *46*, 10810.

(11) For some representative references, see:(a) Harden, N. C.; Bolcar, M. A.; Wernsdorfer, W.; Abboud, K. A.; Streib, W. E.; Christou, G. *Inorg. Chem.* **2003**, *42*, 7067. (b) Yang, E.-C.; Harden, N.; Wernsdorfer, W.; Zakharov, L.; Brechin, E. K.; Rheingold, A. L.; Christou, G.; Hendrickson, D. N. *Polyhedron* **2003**, *22*, 1857. (c) Boskovic, C.; Brechin, E. K.; Streib, W. E.; Folting, K.; Bollinger, J. C.; Hendrickson, D. N.; Christou, G. *J. Am. Chem. Soc.* **2002**, *124*, 3725. (d) Murugesu, M.; Wernsdorfer, W.; Abboud, K. A.; Christou, G. *Polyhedron* **2005**, *24*, 2894. (e) Murugesu, M.; Mishra, A.; Wernsdorfer, W.; Abboud, K. A.; Christou, G. *Polyhedron* **2006**, *25*, 613. (f) Foguet-Albiol, D.; O'Brien, T. A.; Wernsdorfer, W.; Moulton, B.; Zaworotko, M. J.; Abboud, K. A.; Christou, G. *Angew. Chem., Int. Ed.* **2005**, *44*, 897. (g) Murugesu, M.; Wernsdorfer, W.; Abboud, K. A.; Christou, G. *Angew. Chem., Int. Ed.* **2005**, *44*, 892.

(12) Yoo, J.; Brechin, E. K.; Yamaguchi, A.; Nakano, M.; Huffman, J.; Maniero, A.; Brunel, L.; Awaga, K.; Ishimoto, H.; Christou, G.; Hendrickson, D. *Inorg. Chem.* **2000**, *39*, 3615.

(13) Boskovic, C.; Wernsdorfer, W.; Folting, K.; Huffman, J. C.; Hendrickson, D. N.; Christou, G. *Inorg. Chem.* **2002**, *41*, 5107.

(14) Murugesu, M.; Habrych, M.; Wernsdorfer, W.; Abboud, K. A.; Christou, G. *J. Am. Chem. Soc.* **2004**, *126*, 4766.

Experimental Section

Syntheses. All manipulations were performed under aerobic conditions using chemicals as received. ***Caution!*** *Although no such behavior was observed during the present work, azide salts are potentially explosive; such compounds should be synthesized and used in small quantities, and treated with utmost care at all times.*

$[Mn_{25}O_{18}(OH)_2(N_3)_{12}(pdm)_6(pdmH)_6]Cl_2$ (1). A stirred, pale brown slurry of $MnCl_2 \cdot 4H_2O$ (0.15 g, 0.75 mmol), $pdmH_2$ (0.34 g, 2.5 mmol), and NaN_3 (0.16 g, 2.5 mmol) in MeCN/MeOH (20/10 mL) was treated with NMe_4OH (0.10 mL, 0.25 mmol), which resulted in a dark brown solution. The stirring was discontinued, and the solution maintained undisturbed at room temperature. Black crystals of $[Mn_{25}O_{18}(OH)_2(N_3)_{12}(pdm)_6(pdmH)_6]Cl_2 \cdot 12MeCN$ (**1**·12MeCN) slowly grew over a few weeks. When crystallization was judged complete, the crystals were collected by filtration, washed with a little cold MeCN/MeOH, and dried in vacuo. The yield was ~30%. Vacuum-dried material analyzed as solvent-free. Anal. Calcd (Found) for $C_{84}H_{92}Cl_2Mn_{25}N_{48}O_{44}$: C 25.72 (26.01), H 2.36 (2.68), N 17.14 (17.15) %. The crystallographic sample was maintained in mother liquor to avoid solvent loss. Vacuum-dried material is slightly hygroscopic, and it was used for elemental analysis and magnetic studies as soon as possible after drying.

X-ray Crystallography. Diffraction data were collected at 173 K on a Siemens SMART PLATFORM equipped with a CCD area detector and a graphite monochromator utilizing Mo Kα radiation ($\lambda = 0.71073$ Å). A suitable crystal (approximate dimensions 0.17 × 0.17 × 0.06 mm) was attached to the tip of a glass capillary and transferred to the goniostat, where it was cooled for characterization and data collection. Cell parameters were refined using up to 8192 reflections. A full sphere of data (1850 frames) was collected using the ω-scan method (0.3° frame width). The first 50 frames were remeasured at the end of data collection to monitor instrument and crystal stability (maximum correction on I was <1%). Absorption corrections by integration were applied based on measured indexed crystal faces. The structure was solved by direct methods in SHELXTL6,[15] and refined using full-matrix least-squares. The non-H atoms were treated anisotropically, whereas the H atoms were placed in ideal, calculated positions, and refined as riding on their respective C atoms. Unit cell parameters and structure solution and refinement data are listed in Table 1.

The asymmetric unit consists of half a Mn_{25} cluster, a Cl^- anion (disordered equally over two very close sites), and six MeCN solvent molecules. The latter were disordered and could not be modeled properly; thus program SQUEEZE,[16] a part of the PLATON package of crystallographic software, was used to calculate the solvent disorder area and remove its contribution to the overall intensity data. A total of 929 parameters were refined in the final cycles of refinement on F^2 using 9419 reflections with $I > 2\sigma(I)$ to yield R_1 and wR_2 of 5.55 and 15.31%, respectively.

Other Studies. Elemental analyses (C, H, N) were performed by the in-house facilities of the University of Florida Chemistry Department. Infrared spectra in the 400−4000 cm^{-1} range were recorded in the solid state (KBr pellets) on a Nicolet Nexus 670 FTIR spectrometer. Variable temperature direct current (dc) magnetic susceptibility data down to 1.8 K were collected using a Quantum Design MPMS-XL SQUID magnetometer equipped with a 7 T dc magnet. Pascal's constants were used to estimate the diamagnetic corrections, which were subtracted from the experimental susceptibilities to give the molar magnetic susceptibilities (χ_M). Microcrystalline samples were restrained in eicosane by suspending the solid for 15 min in eicosane maintained at a temperature above its melting point (35−37 °C), and then the temperature was gradually decreased below the melting point to solidify the eicosane while maintaining a random orientation of microcrystallites. Magnetization versus field and temperature data were fit using the program MAGNET.[17] Low-temperature (<1.8 K) hysteresis loop and dc relaxation measurements were performed in Grenoble using an array of micro-SQUIDs.[18] The high sensitivity of this magnetometer allows the study of single crystals of the order of 10 to 500 μm. The field can be applied in any direction by separately driving three orthogonal coils.

High-frequency/high-field EPR (HFEPR) spectroscopic studies on polycrystalline samples were performed at the University of Florida in a 17 T superconducting magnet in the 59−269 GHz frequency range using a Millimeter-wave Vector Network Analyzer (MVNA) described elsewhere.[19] The samples were cooled at 10 K/min under 1 atm of He gas. Temperature control was achieved within an Oxford Instruments variable-flow cryostat situated within the 17 T magnet. The MVNA's superheterodyne receiver operates at high frequencies (~34 MHz), thus eliminating the need for field modulation. Consequently, all EPR data presented in this paper correspond to pure absorption, rather than the derivative signals more usually associated with HFEPR measurements. An oversized cylindrical cavity was employed to enhance the sensitivity of the measurement. This provides an added benefit of allowing automatic frequency control using the out-of-phase signal returned from the cavity as a reference. In this way, the MVNA frequency remains locked to the cavity. Such a procedure eliminates any mixing of the dissipative and dispersive response of the sample, thus ensuring that reliable EPR lineshapes are obtained. As will be seen below, this represents an important factor in the present investigation.

Table 1. Crystallographic Data for Complex **1**·12MeCN

formula[a]	$C_{108}H_{128}Cl_2Mn_{25}N_{60}O_{44}$
formula wt, g/mol[a]	4415.1
crystal system	triclinic
space group	$P\bar{1}$
a, Å	15.8921(8)
b, Å	16.5027(8)
c, Å	17.2565(8)
α, deg	98.881(2)
β, deg	99.923(2)
γ, deg	117.003(2)
volume, Å^3	3830.0(3)
Z	1
ρ_{calc}, g/cm^3	1.914
μ, mm^{-1}	2.109
T, K	173(2)
λ, Å [b]	0.71073
data/restraints/parameters	17066/0/929
goodness-of-fit on F^2[c]	0.952
final *R* indices [$I > 2\sigma(I)$] [d,e]	R1 = 0.0555, wR2 = 0.1531
largest diff. peak and hole	0.913 and −1.228 e/Å^3

[a] Excluding solvate molecules. [b] Graphite monochromator. [c] Goodness-of-fit = $[\sum[w(F_o^2 - F_c^2)^2]/N_{obs} - N_{para})]^{1/2}$; all data. [d] $R1 = \sum||F_o| - |F_c||/\sum|F_o|$. [e] $wR2 = [\sum[w(F_o^2 - F_c^2)^2]/\sum[w(F_o^2)^2]]^{1/2}$, $w = 1/[\sigma^2(F_o^2) + (0.2P)^2]$, where $P = (F_o^2 + 2F_c^2)/3$.

(15) *SHELXTL-Plus*, V5.10; Bruker Analytical X-Ray Systems: Madison, WI.
(16) Van der Sluis, P.; Spek, A. L. *Acta Crystallogr., Sect. A: Found. Crystallogr.* **1990**, *A46*, 194.
(17) Davidson, E. *MAGNET*; Indiana University at Bloomington: IN, 1999.
(18) Wernsdorfer, W. *Adv. Chem. Phys.* **2001**, *118*, 99.
(19) (a) Takahashi, S.; Hill, S. *Rev. Sci. Instrum.* **2005**, *76*, 023114. (b) Mola, M.; Hill, S.; Goy, P.; Gross, M. *Rev. Sci. Instrum.* **2000**, *71*, 186.

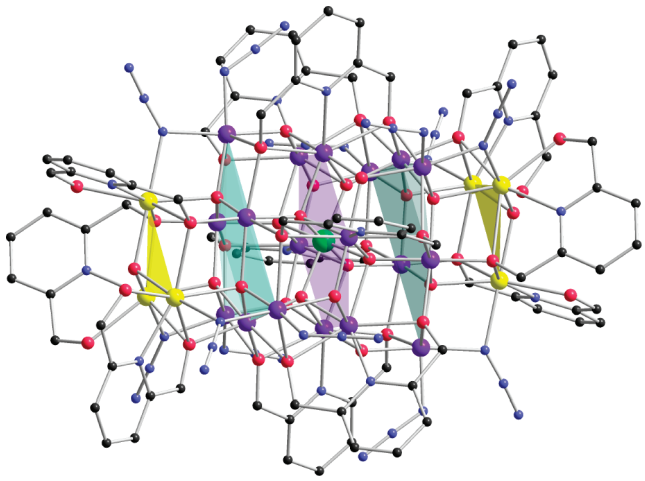

Figure 1. Oak Ridge Thermal Ellipsoid Plot (ORTEP) representation of the complete cation of complex **1** at the 50% probability level and showing the ABCBA layer structure; all H atoms have been omitted for clarity. Mn^{IV} green, Mn^{III} violet-blue, Mn^{II} yellow, N blue, O red, C gray.

Results and Discussion

Syntheses. The synthesis of complex **1** involves the oxidation of Mn^{II} by atmospheric O_2 under the prevailing basic conditions. Thus, a stirred, pale brown slurry of $MnCl_2 \cdot 4H_2O$, $pdmH_2$, and NaN_3 in a 3:10:10 molar ratio in MeCN/MeOH (2:1 v/v) quickly gave a dark brown solution on addition of 1 equiv of NMe_4OH; from this undisturbed solution slowly grew black X-ray quality crystals of **1**·12MeCN in ~30% yield. The reaction is clearly very complicated, likely involving several species in equilibrium, and the crystallization of **1** directly from the reaction solution is doubtless beneficial in providing pure material. In all cases, the filtrates are still colored, but we did not attempt to increase the yield by addition of Et_2O or other co-solvent, being happy to settle for a nonoptimized but good yield of pure, highly crystalline material. The formation of **1** is summarized in eq 1.

$$25Mn^{2+} + 12pdmH_2 + 12N_3^- + 10OH^- + 5O_2 \rightarrow [Mn_{25}O_{18}(OH)_2(N_3)_{12}(pdm)_6(pdmH)_6]^{2+} + 26H^+ \quad (1)$$

The product was isolated as soon as crystallization was judged complete (1−2 weeks) to avoid contamination by the NaCl that deposits at longer times. The NaCl would form rapidly in neat MeCN for separation, but significant amounts of MeOH are essential to increase the solubility of $MnCl_2 \cdot 4H_2O$ and NaN_3 and thus allow the reaction to proceed at a significant rate. The MeCN/MeOH ratio of 2:1 was the successful compromise. When the reaction was carried out in neat MeOH, no Mn product crystallized directly from the brown solution, and no clean product was obtained on addition of a second solvent. If NMe_4OH is omitted from the reaction, the reaction still turns brown but at a much slower rate, presumably facilitated by the weakly basic properties of the N_3^- ion, and the yield of product is much less (at least within the time periods that avoid significant NaCl formation).

Description of the Structure. The structure of complex **1** and its core are shown in Figures 1 and 2. Selected interatomic distances are listed in Table 2. Complex **1**·12MeCN crystallizes in the triclinic space group $P\bar{1}$. The Mn_{25} cation has crystallographic C_i but virtual S_6 symmetry, the C_3 axis being the long axis of the barrel-like structure. The Mn oxidation states were determined qualitatively by inspection of metric parameters and detection of Mn^{III} Jahn−Teller (JT) elongation axes and were confirmed quantitatively by the bond valence sum (BVS) calculations shown in Table 3. These establish the complex to be mixed- and trapped-valence, with a $Mn^{II}_6Mn^{III}_{18}Mn^{IV}$ oxidation level depicted as different colors in Figures 1 and 2.

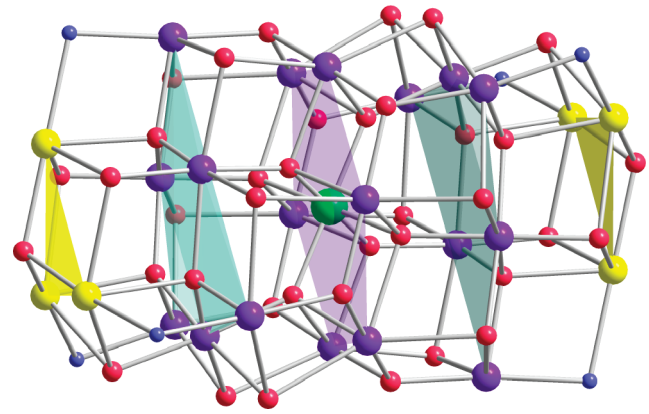

Figure 2. Centrosymmetric barrel-shaped core of the cation of complex **1** emphasizing the ABCBA layer structure.

Table 2. Selected Interatomic Distance (Å) and Angle (deg) Ranges in Complex **1**

parameter	distances
$Mn^{II} \cdots Mn^{II}$	3.416(5)−3.456(3)
$Mn^{II} \cdots Mn^{III}$	3.232(3)−3.387(8)
$Mn^{III} \cdots Mn^{III}$	3.081(5)−3.693(2)
$Mn^{III} \cdots Mn^{IV}$	3.091(4)−3.0945(8)
$Mn^{IV}-\mu_4\text{-}O^{2-}$	1.882(5)−1.888(4)
$Mn^{III}-\mu_4\text{-}O^{2-}$	1.887(4)−2.172(3)
$Mn^{III}-\mu_3\text{-}O^{2-}$	1.874(4)−1.933(5)
$Mn^{III}-\mu_3\text{-}OR^-$	1.876(4)−2.360(5)
$Mn^{II}-\mu_4\text{-}O^{2-}$	2.170(5)−2.201(5)
$Mn^{II}-\mu_3\text{-}OR^-$	2.375(6)−2.471(6)
$Mn^{II}-\mu_3\text{-}OH^-$	2.112(4)−2.122(4)
$Mn^{III}-\mu\text{-}N_{azide}$	1.995(6)−2.016(6)
$Mn^{II}-\mu\text{-}N_{azide}$	2.204(10)−2.239(6)

Table 3. Bond Valence Sums for the Mn Atoms in Complex **1**[a]

atom	Mn^{II}	Mn^{III}	Mn^{IV}	atom	Mn^{II}	Mn^{III}	Mn^{IV}
Mn(1)	1.98	1.84	1.88	Mn(8)	3.22	2.95	3.10
Mn(2)	1.95	1.82	1.85	Mn(9)	3.18	2.91	3.05
Mn(3)	3.26	3.03	3.10	Mn(10)	4.37	4.00	4.20
Mn(4)	2.03	1.90	1.93	Mn(11)	3.18	2.93	3.04
Mn(5)	3.13	2.94	2.97	Mn(12)	3.16	2.92	3.02
Mn(6)	3.21	2.93	3.08	Mn(13)	3.15	2.96	2.99
Mn(7)	3.09	2.91	2.93				

[a] The underlined value is the one closest to the charge for which it was calculated. The formal oxidation state of the atom is the nearest whole number to the underlined value.

The core is held together by twelve μ_4-O^{2-}, six μ_3-O^{2-} and two μ_3-OH^- ions, as well as six μ-N_3^- groups and the deprotonated alkoxide arms of pdm^{2-} and $pdmH^-$ groups. The core can be dissected into five parallel layers of three types with an **ABCBA** arrangement (Figure 3). Layer **A** is a Mn^{II}_3 triangular unit (Mn1, Mn2, Mn4) with a capping μ_3-OH^- ion; layer **B** is a Mn^{III}_6 triangle (Mn3, Mn5, Mn6, Mn7, Mn8, Mn9) that can be described as three corner-fused Mn^{III}_3

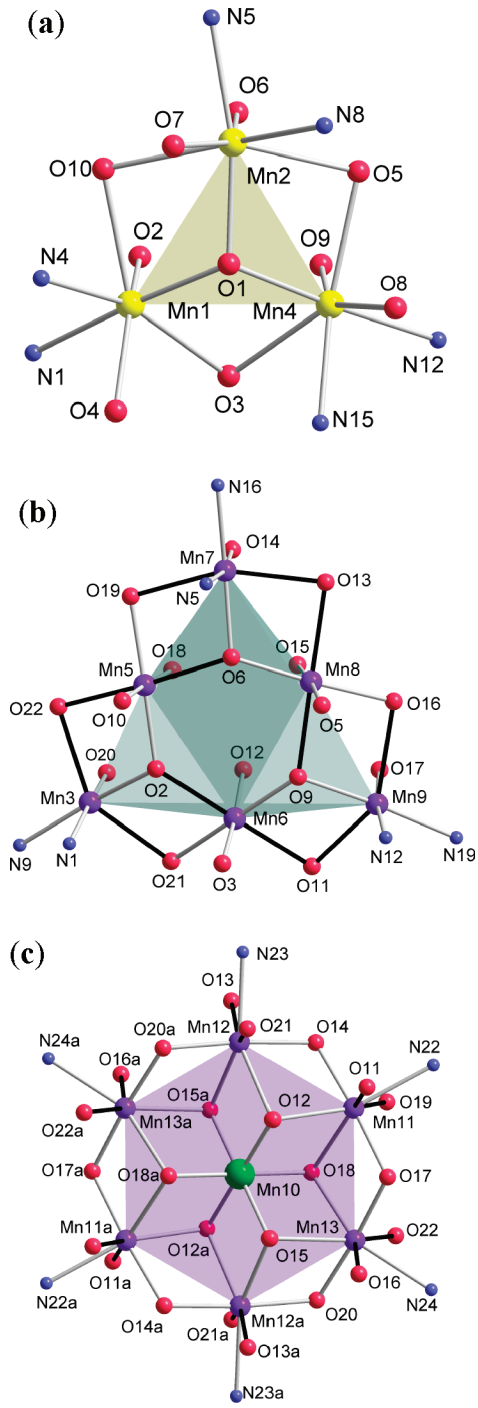

Figure 3. Labeled representations of the three types of Mn_x layers in the cation of **1** shown in Figures 1 and 2. Mn^{IV} green, Mn^{III} violet-blue, Mn^{II} yellow, O red, N blue.

triangular units each capped by a μ_3-O^{2-} ion; and layer **C** is a Mn^{III}_6 hexagon (Mn11, Mn12, Mn13, Mn11a, Mn12a, Mn13a) at the center of which is held the Mn^{IV} ion (Mn10) by six bridging O^{2-} ions. Layer **C** can alternatively be described as six edge-fused $Mn_3(\mu_3\text{-}O^{2-})$ triangular units and is reminiscent of the well-known Anderson-type structure[20] seen in some discrete Mn_7 complexes such as in $[Mn_7(teaH)_3(tea)_3]^{2+}$,[21] $[Mn_7(OH)_3(hmp)_9Cl_3]^{2+}$,[11a] and $[Mn_7(N_3)_6(mda)_6]^{-}$ and $[Mn_7(N_3)_6(teaH)_6]^{-}$.[5] Each layer is linked to its neighboring layers by a combination of oxide, alkoxide, and/or azide bridging groups. The six pdm^{2-} groups are triply

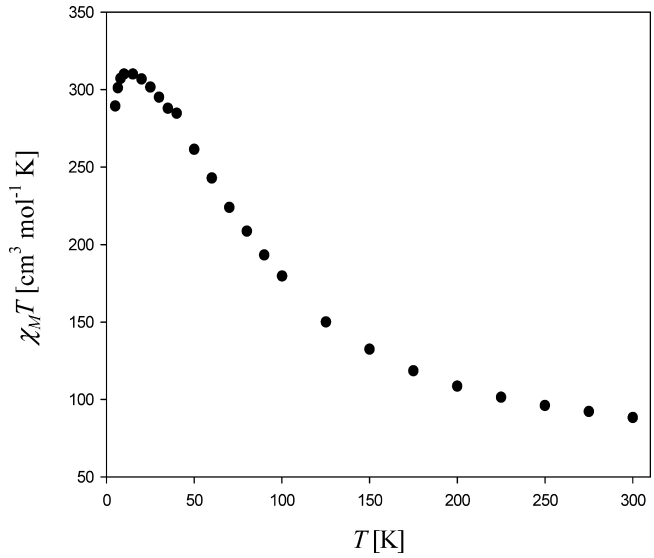

Figure 4. Plot of $\chi_M T$ vs T for complex **1**.

chelating to a Mn^{III} atom of central layer **C**, with each of their deprotonated alkoxide arms bridging to two Mn^{III} atoms of layer **B**; the pdm^{2-} are thus $\eta^3{:}\eta^1{:}\eta^3{:}\mu_5$. The six $pdmH^-$ groups are tridentate chelates to each Mn^{II} atom of layer **A**, with their one deprotonated alkoxide arm bridging to another Mn^{II} in layer **A** and a Mn^{III} in layer **B**; the $pdmH^-$ are thus $\eta^1{:}\eta^1{:}\eta^3{:}\mu_3$. There are six μ-N_3^- groups bridging each Mn^{II} of layer **C** with a Mn^{III} in layer **B**, and the six remaining azides are terminally bound to Mn^{III} atoms of layer **B**. The two Cl^- anions are strongly hydrogen-bonded at each end of the molecule to a μ_3-OH^- ion ($O\cdots Cl \approx 3.16$ Å) and the OH atom O7 of a $pdmH^-$ group ($O\cdots Cl \approx 3.05$ Å). There are no significant intermolecular H-bonds.

The overall barrel shape of the cation is emphasized in the space-filling plots of Figures S1 and S2 (Supporting Information); it has a length of ~19.7 Å and a diameter of ~15.8 Å, excluding H atoms. The voids between Mn_{25} molecules contain the badly disordered MeCN molecules, which do not negatively impact the crystallographic refinement of the structure but have an important effect on the magnetic properties, which are sensitive to the precise environment of the molecules (vide infra).

dc Magnetic Susceptibility Studies. Variable-temperature, solid-state dc magnetic susceptibility (χ_M) data were collected on powdered, microcrystalline samples of complex **1** in the 5.0−300 K range in a 1 kG (0.1 T) field. $\chi_M T$ steadily increases from 88.4 cm^3 K mol^{-1} at 300 K to a maximum of 310 cm^3 K mol^{-1} at 15 K, before decreasing slightly to 289 cm^3 K mol^{-1} at 5.0 K (Figure 4). The 300 K value is slightly higher than the 82.13 cm^3 K mol^{-1} expected if there were no interactions between the Mn ions. The data strongly suggest a very large ground-state spin, with the 5 K value indicating an S in the ${}^{47}/_{2}$−${}^{53}/_{2}$ range, depending on g. For such a large molecule, it is clearly unfeasible to experimentally determine the individual pairwise exchange constants

(20) Hasenknopf, B.; Delmont, R.; Herson, P.; Gouzerh, P. *Eur. J. Inorg. Chem.* **2002**, 1081.
(21) Pilawa, B.; Kelemen, M. T.; Wanka, S.; Geisselmann, A.; Barra, A. L. *Europhys. Lett.* **1998**, *43*, 7.

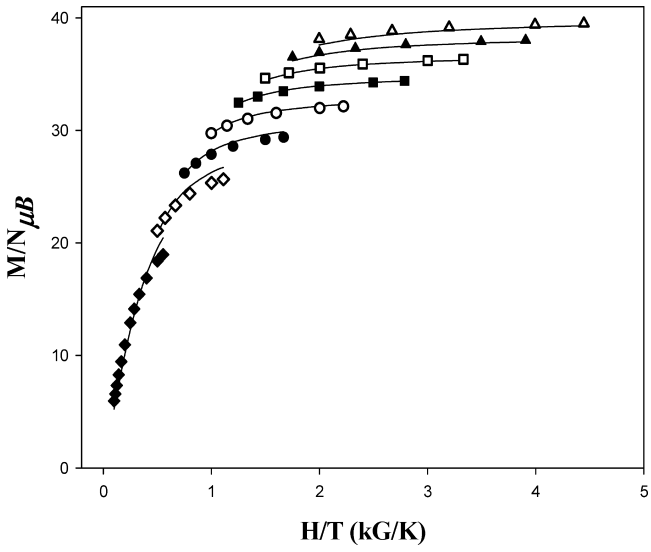

Figure 5. Plot of the reduced magnetization $M/N\mu_B$ vs H/T for complex **1** at fields of 0.1 (◆), 0.2 (◇), 0.3 (●), 0.4 (○), 0.5 (■), 0.6 (□), 0.7 (▲) and 0.8 (△) T. The solid lines are the fit of the data; see the text for the fit parameters.

J_{ij} between Mn_iMn_j pairs, and so we concentrated only on identifying the ground state of the molecule, which was accomplished by collecting variable-temperature and -field magnetization (M) data in the 1.8−4.0 K and 0.1−7.0 T ranges. Attempts to fit the data were made using the program MAGNET,[17] which diagonalizes the spin Hamiltonian matrix assuming only the ground state is populated, incorporates axial anisotropy ($D\hat{S}_z^2$) and Zeeman terms, and employs a full powder average.[22] The corresponding spin Hamiltonian, $\hat{H}$, is given by eq 2,

$$\hat{H} = D\hat{S}_z^2 + g\mu_B\mu_0\hat{S}\cdot H \qquad (2)$$

where D is the axial ZFS constant, μ_B is the Bohr magneton, and μ_0 is the vacuum permeability. The last term in eq 2 is the Zeeman energy associated with an applied magnetic field. However, a good fit could not be obtained using data up to 7 T. This was as expected for a very high nuclearity complex, and especially for one containing multiple Mn^{II} atoms, which give very weak exchange couplings and thus small energy separations between spin states.[8] Both factors will result in a high density of low-lying excited states, which can prevent a good fit because (i) it is difficult to depopulate excited states sufficiently, and/or (ii) the applied dc field will cause the approach and even the crossing of excited state M_S levels with those of the ground state; either one or both will preclude the fitting model from being successful. As reported on previous occasions,[3−6,11,23] we can (usually) circumvent such problems by using a combination of very low temperature data and small fields. Thus, the data for fields only up to 0.8 T and in the 1.8 to 4.0 K range are plotted as reduced magnetization ($M/N\mu_B$) versus H/T in Figure 5, and we now obtained a good fit of the data (solid line in Figure 5) with $S = {}^{51}/_{2}$, $D = -0.020(2)$ cm^{-1}, and $g = 1.87(3)$. When data collected at fields >0.8 T were included, a satisfactory fit could not be obtained (Figure S4, Supporting Information), suggesting that the main fitting problem is the dc field-induced crossing of the M_S levels of excited states with S values greater than that of the ground state, which is consistent with the many antiferromagnetic interactions expected within **1**. The presence of low-lying excited states is clearly visible in plots of $M/N\mu_B$ versus H/T and versus H (Figure S5, Supporting Information) using only data collected at 1.8 K; these show an absence of saturation at high fields and only a steadily increasing $M/N\mu_B$ consistent with population of excited state M_S levels, as above.

Note that in our preliminary report[14] we had obtained fit parameters of $S = {}^{51}/_{2}$, $D = -0.022$ cm^{-1}, and $g = 1.72$ for **1**. The unusually low g value was worrisome, and we have now tracked down the problem as being due to the slightly hygroscopic nature of vacuum-dried **1**, which we had not originally realized, and its influence on the apparent molar amounts of **1** used for the magnetization measurements. Thus, for this report, multiple measurements have been made on samples freshly vacuum-dried, and these give the fit parameters above with a more reasonable $g = 1.87(3)$. This is likely still lower than the true value, and it is well-known that fits of powder magnetization measurements are not the best way to determine an accurate g value. EPR spectroscopy is a more accurate way of obtaining g (vide infra).

The obtained negative D value for **1** is rather small in absolute magnitude compared with other Mn clusters such as $[Mn_{12}O_{12}(O_2CR)_{16}(H_2O)_4]$[10] and $[Mn_4O_3X(O_2CR)_3(dbm)_3]$[24] (X = Cl^-, Br^-, F^-, etc; dbm^- is the anion of dibenzoylmethane) whose D values are in the ∼ −0.3 to −0.6 cm^{-1} range. This is despite **1** containing eighteen Jahn−Teller (JT) distorted Mn^{III} atoms, whose anisotropies represent the major contribution to the overall molecular anisotropy. However, inspection of the relative orientation of Mn^{III} JT elongation axes in **1** reveals that the six JT axes of the central layer **C** are roughly parallel to each other and perpendicular to the layer plane, and that the twelve remaining JT axes in the two **B** layers separate into two sets of six roughly perpendicular to each other and to those in layer **C**. Thus, there is a roughly symmetric distribution of JT axis orientations in the molecule. Because the molecular anisotropy is the tensorial projection of the individual single-ion anisotropies onto the molecular anisotropy (z) axis, there is expected to be a major cancelation and a resulting small molecular anisotropy,[3a−c,4d,7] that is, a small $|D|$ value, as found. This is not the case for the Mn_{12} and Mn_4 complexes, whose eight and three Mn^{III} JT axes, respectively, are aligned far from perpendicular and thus give a significant net molecular anisotropy.

(22) Yoo, J.; Yamaguchi, A.; Nakano, M.; Krzystek, J.; Streib, W. E.; Brunel, L.-C.; Ishimoto, H.; Christou, G.; Hendrickson, D. N. *Inorg. Chem.* **2001**, *40*, 4604.

(23) Soler, M.; Wernsdorfer, W.; Folting, K.; Pink, M.; Christou, G. *J. Am. Chem. Soc.* **2004**, *126*, 2156.

(24) (a) Wemple, M. W.; Adams, D. M.; Hagen, K. S.; Folting, K.; Hendrickson, D. N.; Christou, G. *J. Chem. Soc., Chem. Commun.* **1995**, 1591. (b) Wemple, M. W.; Tsai, H.-L.; Folting, K.; Hendrickson, D. N.; and Christou, G. *Inorg. Chem.* **1993**, *32*, 2025. (c) Aliaga-Alcalde, N.; Edwards, R. S.; Hill, S. O.; Wernsdorfer, W.; Folting, K.; Christou, G. *J. Am. Chem. Soc.* **2004**, *126*, 12503; and references cited therein.

The $S = {}^{51}/_{2}$ ground state and negative D value suggested that **1** might be an SMM. The upper limit to the relaxation barrier is $(S^2 - {}^{1}/_{4})|D|$ for a half-integer spin, or only 13 cm^{-1} for **1**, but the actual (or effective) barrier (U_{eff}) will be less because of quantum tunneling of the magnetization (QTM)[25] through the barrier via higher energy M_S levels. The large S of ${}^{51}/_{2}$ is beneficial for obtaining a large barrier but the unfortunately small D of -0.020 cm^{-1} counteracts this, and the calculated U of 13 cm^{-1} is consequently small. Nevertheless, such a value is still large enough to suggest that complex **1** might function as an SMM at a low enough temperature. We thus decided to investigate this complex using alternating current (ac) magnetic susceptibility measurements.

ac Magnetic Susceptibility Studies. The ac studies were performed in a 3.5 G ac field oscillating at frequencies (ν) in the 50−1000 Hz range to probe the magnetization relaxation dynamics of complex **1**. Such studies were a source of two important pieces of information: (i) whether **1** is an SMM; and (ii) confirmation of the magnitude of its ground-state S value.

If there is a significant barrier (vs kT) to magnetization relaxation, then at low enough temperature the magnetization of **1** will not be able to relax fast enough to keep in-phase with the oscillating ac field, and an out-of-phase (χ_M'') ac signal will be observed whose exact position will be frequency-dependent; such a superparamagnet-like behavior is necessary but not sufficient proof of an SMM.[26] The obtained χ_M'' versus T plot is shown in Figure 6 (bottom), and it exhibits a nonzero, frequency-dependent χ_M'' signal below ~3 K. These are clearly the "tails" of peaks whose maxima lie at temperatures <1.8 K, the operating minimum of our SQUID magnetometer. As expected, the increase in χ_M'' is accompanied by a similarly frequency-dependent drop in the in-phase (χ_M') ac signal when plotted as $\chi_M'T$ versus T in Figure 6 (top).

The absence of a dc field in the ac experiment avoids the Zeeman complications mentioned above, and thus the in-phase signal provides an excellent additional and independent method for determining the ground-state S value. When plotted as $\chi_M'T$ versus T as in Figure 6 (top), and in the absence of an out-of-phase signal, the plot will be essentially temperature-independent at low T if only the ground state is populated, but will be distinctly sloping if excited states are still being depopulated with decreasing temperature.[3d−g,4d,11f,g,26,27] The $\chi_M'T$ versus T plot of Figure 6 (top) shows a strong signal that decreases with decreasing T. It is likely that the somewhat steeper decrease below ~5 K is due to weak intermolecular exchange interactions, both dipolar and superexchange, especially given the large S of the molecule, and the shallower decrease at higher T because of depopulation of excited states with S greater than that of the ground state; this picture is also consistent with the conclusions from the dc magnetization fits described earlier. The first and most important conclusion to be drawn from these ac data, which show a large $\chi_M'T$ at low T in the ~300 cm^3 K mol^{-1} range (i.e., similar to the dc data), is that the large dc $\chi_M T$ values at low T of Figure 4 were not an artifact of the applied dc field, that is, the ground-state S really is large.

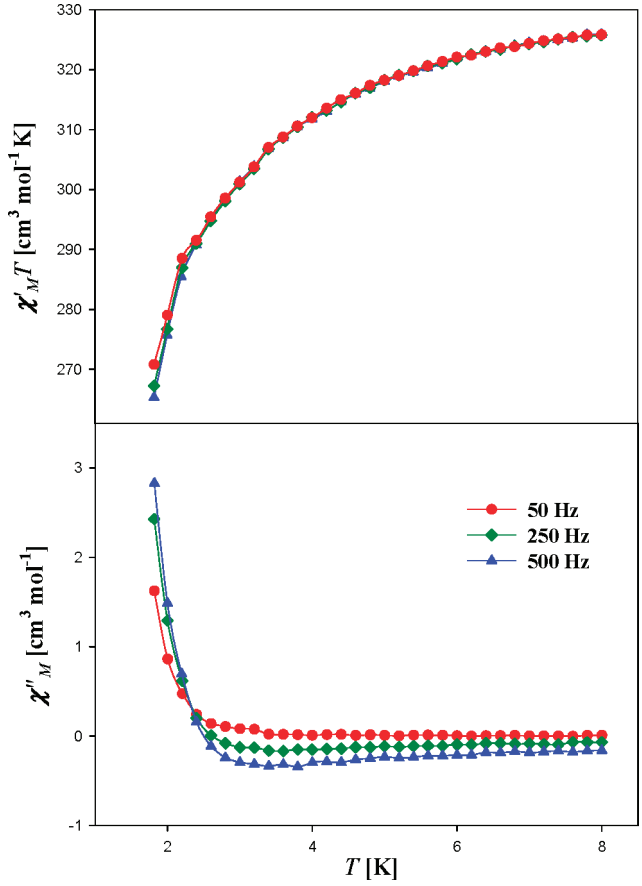

Figure 6. Plot of in-phase ac susceptibility signals (χ_M', plotted as $\chi_M'T$ vs T, top) and out-of-phase ac magnetic susceptibility (χ_M'') vs T for complex **1** at the indicated ac frequencies. The solid lines are visual aids.

Extrapolation of $\chi_M'T$ in Figure 6 (top) from values above ~5 K to avoid complications from effects such as intermolecular interactions and ZFS at lower temperatures gives a value of ~300−310 cm^3 K mol^{-1}, which indicates a ground-state spin for the molecule in the $S = {}^{49}/_{2}$−${}^{53}/_{2}$ range, depending on g, comparable to the conclusion of the dc magnetization fits. A value of, say, 305 cm^3 K mol^{-1} is consistent with the following S (g) combinations: ${}^{49}/_{2}$ (1.98), ${}^{51}/_{2}$ (1.90), and ${}^{53}/_{2}$ (1.83); all these are reasonable for Mn, since g is expected to be slightly less than 2.0.[8a] We conclude

(25) (a) Friedman, J. R.; Sarachik, M. P.; Tejada, J.; Ziolo, R. *Phys. Rev. Lett.* **1996**, *76*, 3830. (b) Thomas, L.; Lionti, L.; Ballou, R.; Gatteschi, D.; Sessoli, R.; Barbara, B. *Nature* **1996**, *383*, 145. (c) Wernsdorfer, W.; Sessoli, R. *Science* **1999**, *284*, 133. (d) Soler, M.; Wernsdorfer, W.; Folting, K.; Pink, M.; Christou, G. *J. Am. Chem. Soc.* **2004**, *126*, 2156. (e) Canneschi, A.; Ohm, T.; Paulsen, C.; Rovai, D.; Sangregorio, C.; Sessoli, R. *J. Magn. Magn. Mater.* **1998**, *177*, 1330. (f) Barbara, B.; Wernsdorfer, W.; Sampaio, L. C.; Park, J. G.; Paulsen, C.; Novak, M. A.; Ferrer, R.; Mailly, D.; Sessoli, R.; Caneschi, A.; Hasselbach, K.; Benoit, A.; Thomas, L. *J. Magn. Magn. Mater.* **1995**, *140*, 1825.

(26) (a) Moushi, E.; Lampropoulos, C.; Wernsdorfer, W.; Nastopoulos, V.; Christou, G.; Tasiopoulos, A. J. *Inorg. Chem.* **2007**, *46*, 3795. (b) Chakov, N. E.; Wernsdorfer, W.; Abboud, K. A.; Christou, G. *Inorg. Chem.* **2004**, *43*, 5919. (c) Mishra, A.; Tasiopoulos, A. J.; Wernsdorfer, W.; Abboud, K. A.; Christou, G. *Inorg. Chem.* **2007**, *46*, 3105.

(27) Sanudo, E. C.; Wernsdorfer, W.; Abboud, K. A.; Christou, G. *Inorg. Chem.* **2004**, *43*, 4137.

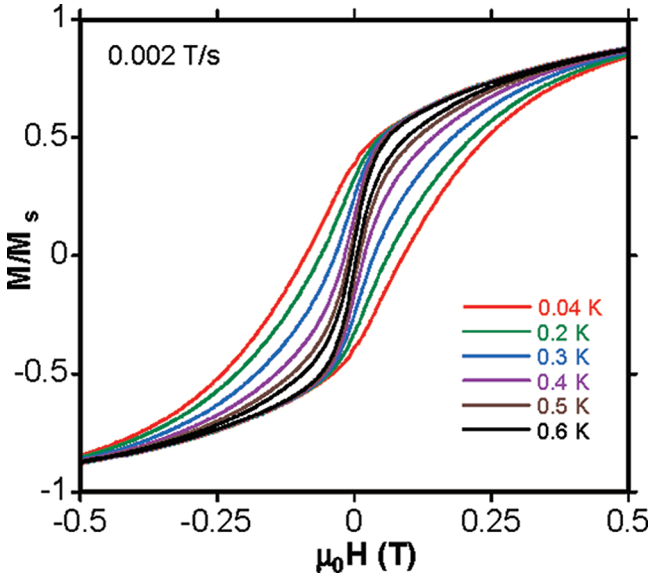

Figure 7. Magnetization (M) vs dc field hysteresis loops for complex **1** at the indicated field scan rates and temperatures. The magnetization is normalized to its saturation value, M_S.

that **1** has an $S = {}^{51}/_{2} \pm 1$ ground state with $g = 1.90 \pm 0.08$, in agreement with the dc magnetization fit values.

Magnetization versus dc Field Hysteresis Studies. To explore further the implication of the ac out-of-phase data that complex **1** might be a SMM, magnetization versus applied dc field scans were carried out using a micro-SQUID apparatus[18] on single crystals of **1**·12MeCN that had been maintained in contact with the mother liquor to avoid solvent loss. Shown in Figure 7 are the results of magnetization (M) versus applied dc field sweep rates at a 0.002 T/s field sweep rate and temperatures in the 0.04−0.6 K range. Hysteresis loops were observed, whose coercivities (widths) increase with decreasing temperature, as expected for the superparamagnet-like properties of a SMM. There is an insignificant scan rate dependence of the coercivity visible at 0.04 K but a small one becomes apparent at 0.3 and 0.4 K (Figure S6, Supporting Information).

The hysteresis loops show no sign of the steps diagnostic of resonant QTM that are visible in the loops of smaller SMMs such as Mn_4 and Mn_{12}, and this is typical of large molecules such as, for example, the Mn_{18},[3f] Mn_{24},[3d] Mn_{26},[3d] Mn_{30},[23] and Mn_{84}[28] complexes, for which the steps are broadened and smeared out from a distribution of molecular environments caused by, for example, disordered ligands and lattice solvent molecules, especially given the large voids between large molecules that almost always contain significant amounts of solvent of crystallization. Step broadening will also occur from low-lying excited states, and this situation is again common in high nuclearity complexes, as discussed above. In fact, the only exception to date of a large molecule for which well-resolved QTM steps have been observed is a Mn_{22} complex.[29]

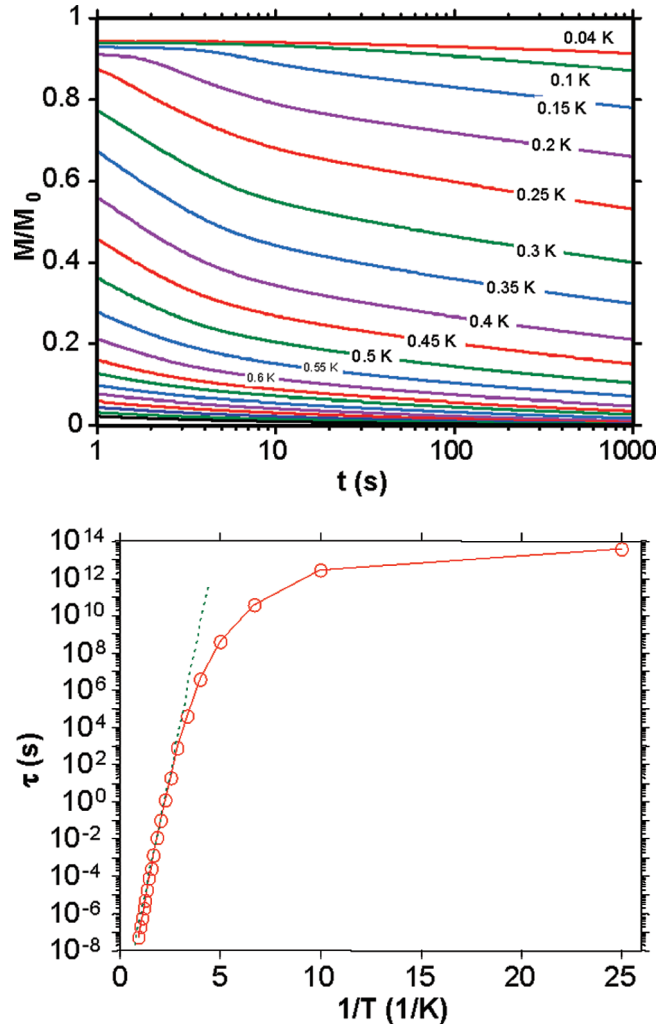

Figure 8. (top) Magnetization (M) vs time decay plots in zero dc field for a single crystal of **1**·12MeCN. The magnetization is normalized to M_0, the initial value at 0.04 K. (bottom) Arrhenius plot of the relaxation time (τ) vs $1/T$ for **1**·12MeCN using data from the top figure. The dashed line is the fit of the data in the thermally activated region to the Arrhenius equation; see the text for the fit parameters.

An alternative means of assessing whether QTM is occurring is to monitor the decay of the magnetization with time. The magnetization of **1** was first saturated in one direction at ~5 K with a large dc field, the temperature decreased to a chosen value, the field removed, and the magnetization decay monitored with time. The results are shown in Figure 8 (top) for the 0.04−1.0 K range. This provided magnetization relaxation time (τ) versus temperature data, shown as a τ versus $1/T$ plot in Figure 8 (bottom) based on the Arrhenius relationship of eq 3,

$$\tau = \tau_0 \exp(U_{\text{eff}}/kT) \qquad (3)$$

where τ_0 is the pre-exponential factor, U_{eff} is the mean effective barrier to relaxation, and k is the Boltzmann constant. The fit of the thermally activated region above ~0.35 K, shown as the dashed line in Figure 8 (bottom), gave $U_{\text{eff}} = 8.3$ cm^{-1} (12 K) and $\tau_0 = 3 \times 10^{-12}$ s. The small value of τ_0, smaller than is typical for purely SMM behavior,[2,10,24,25] is likely due to some weak intermolecular interactions and the low-lying excited states; larger clusters

(28) Tasiopoulos, A. J.; Vinslava, A.; Wernsdorfer, W.; Abboud, K. A.; Christou, G. *Angew. Chem., Int. Ed.* **2004**, *43*, 2117.
(29) Brockman, J. T.; Stamatatos, Th. C.; Wernsdorfer, W.; Abboud, K. A.; Christou, G. *Inorg. Chem.* **2007**, *46*, 9160.

often give somewhat smaller τ_0 values.[3,6,11,14,23,28] The mean barrier U_{eff} is thus smaller than the $U = (S^2 - {}^{1}/_{4})|D| = 13$ cm^{-1} calculated with the $S = {}^{51}/_{2}$ and $D = -0.020$ cm^{-1} values obtained from the dc magnetization fit. As stated earlier, U represents the upper limit to the relaxation barrier, but the true barrier U_{eff} is less due to QTM through the barrier between higher energy M_S levels of the $S = {}^{51}/_{2}$ spin manifold. In other words, the system does not have to get to the top of the barrier (i.e., the $M_S = \pm$ 1/2 levels) but instead can tunnel through the barrier at some lower M_S level. At lower temperatures in Figure 8 (bottom), the plot shows only essentially temperature-independent relaxation, as expected for ground-state QTM, that is, the QTM is now only between the lowest-lying $M_S = \pm {}^{51}/_{2}$ levels.

Origin of the Large Ground State S Value. In the spirit of the desire discussed in the Introduction to rationalize the origin of the S values of molecules on the basis of their structures, it is of interest to ask if any simple rationalization of the $S = {}^{51}/_{2}$ ground state can indeed be achieved from the structure of **1**. However, this molecule is simply too complicated, and the answer is "no". Of course, there are several simple, arithmetic ways of getting $S = {}^{51}/_{2}$ from the constituent metals, and one of them was offered in the preliminary report of this work:[14] this is simply to assign the spins of layers **A**, **B**, and **C** as being 15/2, 0, and 21/2, respectively, corresponding to (i) three ferromagnetically coupled Mn^{II} spins in layer **A** giving $S = {}^{15}/_{2}$; (ii) an antiferromagnetically coupled Mn^{III}_6 triangle in layer **B** giving $S = 0$; and (iii) six Mn^{III} spins in layer **C** strongly antiferromagnetically coupled to the central Mn^{IV} spin, and thus aligned parallel to each other, giving $S = {}^{21}/_{2}$. Parallel alignment of the spins of layers **A** and **C** as a result of interactions via Mn ions in layer **B** then predicts a molecular spin of $S = (15/2 + 21/2 + 15/2) = 51/2$. In reality, however, the true situation will be much more complicated and difficult to identify because the structure is the fusion of many Mn_3 triangular units, both within each layer (Figure 3) and between layers (Figure 2). Because most of the exchange interactions are likely to be antiferromagnetic, and of comparable magnitude except for the $Mn^{III}\cdots Mn^{IV}$ ones, extensive spin frustration effects will be operating. As a result, there will almost certainly be intermediate spin alignments at many metal atoms, and the ground-state wave function will thus be too complicated to identify in the absence of computational treatments. The only safe conclusion that appears possible is that the spin of the central layer **C** will be $S = {}^{21}/_{2}$ as a result of the strong $Mn^{III}\cdots Mn^{IV}$ interactions overcoming the $Mn^{III}\cdots Mn^{III}$ interactions within **C** and between **C** and **B**, and thus aligning the six Mn^{III} spins of layer **C** antiparallel to the central Mn^{IV} spin.[8] The resulting $S = {}^{21}/_{2}$ spin of layer **C** would then no doubt represent a significant contribution to the resulting large overall S of the molecule, as will the ferromagnetic interactions expected for Mn_2 pairs bridged by the six end-on-bridging azide groups.[3a−d,7]

High-Frequency Cavity-Based EPR Spectroscopy of Complex 1. To obtain independent confirmation of the SMM behavior of complex **1**, and to obtain an independent assessment of g and D, we have performed high-frequency/high-field EPR (HFEPR) measurements on a portion of the same powder sample used for the ac susceptibility studies shown in Figure 6.

In principle, both the ground-state spin S and the ZFS parameter D can be determined directly via HFEPR experiments. In particular, the D parameter splits the EPR spectrum into $2S$ fine-structure peaks whose spacing depends on the magnitude of D and on the orientation of the applied field relative to the easy axis (z) of the sample; in the true high-field limit ($g\mu_B B \gg DS$), the spacing in field is $D/g\mu_B$ and $D/2g\mu_B$ for applied fields B ($= \mu_0 H$) parallel and perpendicular, respectively, to the z-axis. If D/μ_B is small compared to the EPR linewidths, as is the case for complex **1**, then this fine structure will not be resolved within the EPR spectrum. However, for the case of a powder sample having a significant S, one may expect to see a splitting in the EPR pattern at low temperatures because of the extrema of the parallel (z) and perpendicular (xy) components of the spectrum. The magnitude of this splitting depends both on S and on D. Thus, it is only possible to estimate the product DS in this case, but this nevertheless provides a useful independent verification of the spin value and ZFS parameters obtained from the magnetization measurements. Furthermore, from the shape of the EPR spectrum, one can directly determine the sign of D unequivocally, something which is not so easy to achieve via fits of magnetization data because they tend to yield good fits for parameter sets having both positive and negative D values.

Figure 9 presents experimental spectra recorded at three different microwave frequencies (63.3, 154.2, and 233.3 GHz) and in a range of temperatures between 1.4 and 20 K. The figure displays the signal transmitted through the cavity, and the dips in transmission consequently correspond to absorption within the cavity. Apart from the obvious shift in field, the data for the two highest frequencies are virtually indistinguishable in terms of the temperature dependence of their widths and shapes. This immediately indicates ZFS as the source of the asymmetry observed at the lowest temperatures: note that the 20 K spectrum is very symmetric whereas a shoulder starts to appear on the low-field sides of the peaks at around 10 K, becoming most pronounced at the lowest temperature. The 63.3 GHz data are quite similar, showing a shift in intensity to lower fields upon cooling. Nevertheless, the line shape is a little different from the higher frequency data; we comment further on these differences below. In addition, a weak shoulder can be seen in the 63.3 GHz data at half the field of the main resonance. In fact, this shoulder, which corresponds to a double quantum transition ($g \approx 4$), can be seen in most of the spectra at 15 K if one looks carefully enough.

By repeating such measurements at several significantly different frequencies (i.e., fields), one can begin to deconvolute the various factors affecting the spectra. First of all, by plotting the position in field of the absorption maxima (transmission minima) versus frequency, one can estimate the average Landé g-factor for the complex. Such plots are displayed in Figure 10 for data obtained both at high and

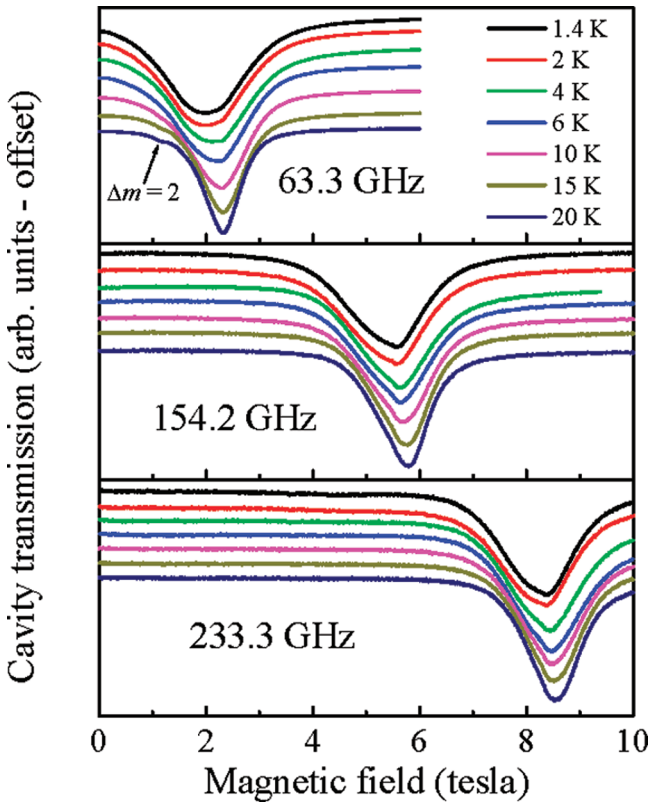

Figure 9. Experimental powder EPR spectra for complex **1** recorded at microwave frequencies of 63.3, 154.2, and 233.3 GHz, and at temperatures in the 1.4 to 20 K range.

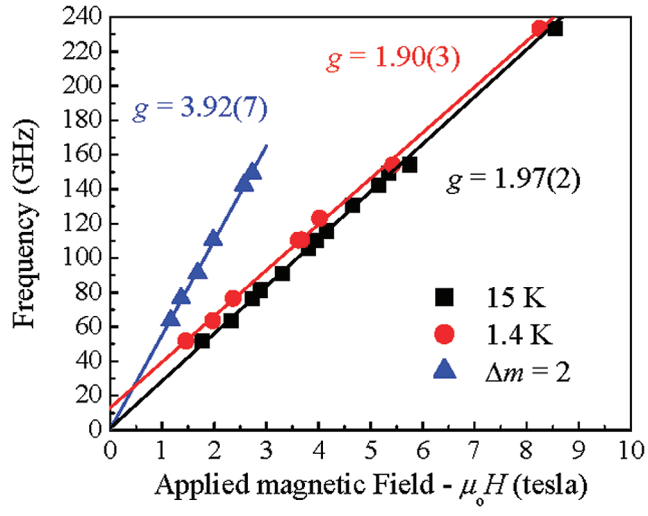

Figure 10. Plots of the field positions of the resonance minima (data points) from spectra such as those in Figure 9 at temperatures of 1.4 and 15 K; the $\Delta m = 2$ double quantum transitions were recorded at 15 K. The solid lines represent linear fits to the data points, from which the Landé *g*-factor was obtained.

low temperatures (the $g \approx 4$ data points were deduced from 15 K data). The higher temperature measurements yield higher average values of $g \approx 1.97(3)$. However, one has to be somewhat careful with these estimates, as the internal fields within the sample will tend to vary from low to high fields because of magnetization of the sample, even at a temperature as high as 15 K. Consequently, the real magnetic induction (B) in the sample will depend in a nonlinear fashion on the applied field $\mu_0 H$. Given the large spin value for the Mn_{25} complex, this could lead to an overestimate of g, since the higher field data points will tend to shift to lower applied fields because of magnetization of the sample; the magnetization can add at most 0.15 T to the applied field ($\mu_0 H$).[30] At lower temperatures, one expects the magnetization to saturate fairly quickly, provided there are no significant changes in the ground-state spin value (see below). In this situation, the effect of the magnetization will simply be to produce a zero-field offset when one plots the resonance positions versus frequency. Indeed, such an offset is apparent from the low-temperature data in Figure 10, although most of the offset is likely due to ZFS (only about 0.15 T, or 4 GHz, could be attributable to the sample magnetization). If one assumes the sample magnetization to be more-or-less constant over the experimental field range, then the slope of the fit to the red data points in Figure 10 should provide a reasonably reliable estimate of the Landé *g*-factor; such a procedure gives a lower value of $g \approx 1.90(3)$. Since we are not exactly sure how good this assumption is, the safest overall conclusion from these combined studies is that the g value is in the 1.90−1.97 range, that is, as expected for Mn complexes, namely, slightly below 2.0.

We next consider the origin of the asymmetry in the spectra observed at the lowest temperatures. One possibility would be *g*-strain, that is, an anisotropic *g*-tensor. However, the widths of the peaks and the position of the low-field shoulder in relation to the main peak appear not to depend noticeably on the applied field strength. This is completely inconsistent with *g*-strain, where the splitting should scale with the field, that is, the splitting should increase by roughly a factor of 4 between the 63.3 and 233.3 GHz data. On the other hand, such a field-independent splitting is fully consistent with ZFS, either with $D < 0$ or $D > 0$. To illustrate the expected behavior for the case of axial ZFS, we have simulated the powder spectrum at 1.4 K for different values of the DS product (in units of 0.46 cm^{-1}), as shown in Figure 11.[31] A Lorentzian line width of 0.5 T is found to give the best overall agreement with the experimental spectra. Such a large line width results in a smearing out of the 2S fine-structure within the spectrum. Nevertheless, one can begin to resolve the parallel (z) and perpendicular (xy) components of the powder spectrum for a DS product of about 0.46 cm^{-1}, that is, a shoulder appears on the low (high) field side of the main peak for negative (positive) D values. Therefore, the fact that we see a shoulder in the experimental spectra indicates a DS product of this order for complex **1**.

Comparisons between the simulations in Figure 11 and the lowest temperature spectra in Figure 9 reveal a negative D value, that is, the weaker shoulder (z component of the spectrum) emerges on the low-field side of the stronger xy component of the spectrum. This supports the earlier conclusion that complex **1** is a SMM. The disappearance of the shoulder upon raising the temperature is connected with

(30) Hill, S.; Maccagnano, S.; Park, K.; Achey, R. M.; North, J. M.; Dalal, N. S. *Phys. Rev. B* **2002**, *65*, 224410.
(31) Jacobsen, C. J. H.; Pederson, E.; Villadsen, J.; Weihe, H. *Inorg. Chem.* **1993**, *32*, 1216; powder EPR simulation program written by H. Weihe, University of Copenhagen, http://sophus.kiki.dk/software/epr/epr.html.

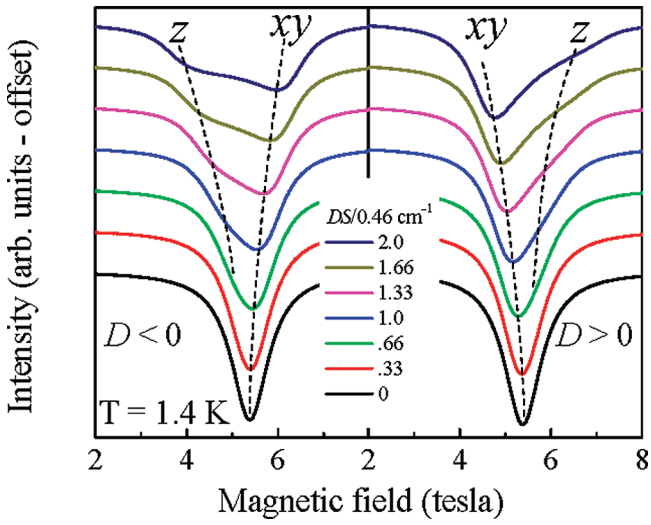

Figure 11. Simulations of the powder spectrum at 1.4 K for different values of the *DS* product (in units of 0.46 cm^{-1}). The appearance of a shoulder on the low (high) field side of the main peak for negative (positive) *D* values, corresponding respectively to parallel (*z*) and perpendicular (*xy*) components of the powder spectrum, indicates a *DS* product of ~ -0.46 cm^{-1}.

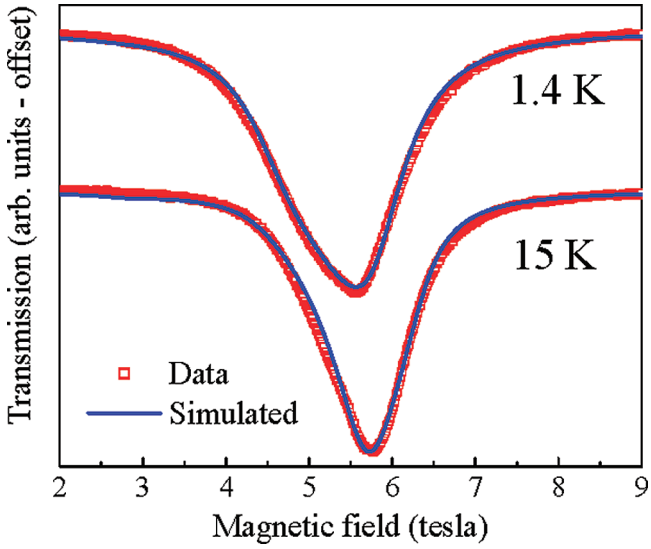

Figure 12. Fits of the 1.4 and 15 K spectra shown in Figure 10.

the population of higher lying levels within the $S = {}^{51}/_{2}$ multiplet, and possibly other low-lying states with $S \neq {}^{51}/_{2}$. This is reflected in fits to the experimental spectra, as shown for the 154.2 GHz data in Figure 12, that is, the low temperature data and simulation exhibit a shoulder, while the high-temperature curves do not. Because the fine-structure of 2*S* lines is not resolved in the spectrum, the least-squares fits to the data were performed by assuming a smaller *S* value of ${}^{9}/_{2}$, that is, we reduced the dimensions of the matrix that had to be diagonalized during each iteration. We verified the quality of the fit by subsequently simulating the spectrum with *S* rescaled to ${}^{51}/_{2}$, while keeping *DS* fixed. No difference can be seen between the $S = {}^{9}/_{2}$ and $S = {}^{51}/_{2}$ simulations for the same *DS* product, thus reaffirming the fact that these studies are sensitive only to *DS* and not *D* or *S* independently.

The actual *DS* value obtained from the fit contains a significant uncertainty. In particular, there is an interdependence between the line width and the obtained *DS* product. In fact, the high temperature data are completely unreliable for obtaining *DS*, though one can always obtain a good fit to the high-temperature data using the *DS* value obtained from fits at low temperature. Nevertheless, we excluded *DS* values obtained from the high-temperature fits in our final analysis. In addition, the quality of the fit for the lowest frequency data is not so good. This can be seen directly by comparing the lineshapes for the 63.3 GHz spectra in Figure 9 with the simulations in Figure 11.

One possible explanation for the poor quality of the fits at low frequencies and fields would be the existence of multiple low-lying states with $S \neq {}^{51}/_{2}$. Indeed, one cannot rule out the possibility that the (approximate) ground-state spin quantum number varies across the field range employed in these HFEPR studies, as also suggested from the fact that the low temperature magnetization does not completely saturate (see Figures 7 and S5, Supporting Information). At the higher fields, one would expect the low-lying spin multiplet with the largest spin value to dominate the EPR spectrum because of its larger Zeeman energy shift. In contrast, at lower fields, several spin multiplets may contribute to the spectrum, thus perhaps explaining the higher quality fits to the high-field data. We note that the various low-lying states probably do not differ significantly in their (approximate) spin quantum numbers. Thus, the *DS* product obtained from these EPR measurements characterizes the average ZFS among the lowest high-spin states. However, one may presume that slight variations in the total spin will not significantly affect the projection of the individual single-ion (mainly Mn^{III}) anisotropies onto the total spin ground state. Not only this, but a rough rule-of-thumb has been established from studies on polynuclear Mn^{III} complexes that, as *S* goes up (down), one expects *D* to go down (up) proportionately.[32] Thus, to a first approximation, it is unlikely that the *DS* product varies significantly between the various low-lying spin multiplets, certainly not within the bounds of the experimental uncertainty of these measurements. But most importantly, these EPR studies unambiguously demonstrate that the splitting of the spectra seen in Figure 9 is indicative of axial ZFS with a negative *D* value.

Taking the averages of the values obtained from the 233.3 and 154.2 GHz fits gives $DS = -0.44(4)$ cm^{-1}. If one assumes that the lowest lying spin multiplet does indeed have $S = {}^{51}/_{2}$, this gives a value of $D = -0.017(2)$ cm^{-1}, in reasonable agreement with the fit of the magnetization data ($D = -0.020(2)$ cm^{-1}).

Conclusions

The amalgamation of $pdmH_2$ and azide in a reaction system involving a simple Mn^{II} reagent has provided access to a new mixed-valence Mn_{25} structural type containing three metal oxidation states, namely $Mn^{II}_{6}Mn^{III}_{18}Mn^{IV}$. The synthesis emphasizes again the ability of alkoxide-containing chelates to foster formation of high nuclearity products, in this case giving, when combined with azide, an interesting Mn_{25} topology comprising five layers in an **ABCBA** ar-

(32) Datta, S.; Hill, S., in preparation.

rangement. Complex **1** has also been found to have a large $S = {}^{51}/_{2} \pm 1$ ground state, as determined by independent dc and ac measurements, as a likely result of a large $S = {}^{21}/_{2}$ spin for the central layer **C**, some ferromagnetic interactions mediated by the end-on bridging azide groups, and spin frustration effects within the many triangular Mn_3 subunits. The $\pm$ 1 uncertainty in the overall S is reasonable: while a difference of ± 1 units is a big one in relative terms when S is small, for example the $S = {}^{9}/_{2}$ of the Mn_4 distorted-cubanes,[24] allowing the ground-state S value to be determined with certainty, the data fits are somewhat less discriminatory when S is much larger at $S = {}^{51}/_{2}$. Nevertheless, the combined dc and ac data obtained and discussed above make us very confident in our conclusion that complex **1** has an $S = {}^{51}/_{2} \pm 1$ ground state.

Because the SMM properties of a molecule depend on it having both a significant S and a significant and negative D, the assessment of the magnitude and sign of D as accurately as possible was also a main aim of this work. Both the magnetization and EPR data independently indicate a small D and are satisfyingly in agreement with a value of $D \sim -0.02$ cm^{-1}; the latter is totally consistent with the structure, namely, the near isotropic distribution of Mn^{III} JT elongation axes. The EPR technique is a particularly powerful, sensitive, and reliable one for such studies and also unequivocally confirms D to be negative in sign, an important conclusion that cannot be reached with safety from magnetization studies on microcrystalline powders alone.

The observed SMM properties of complex **1** have thus been rationalized as arising from a large S and small D, giving an unfortunately small effective barrier of $U_{eff} = 8.3$ cm^{-1} (12 K). Nevertheless, complex **1** is one of the largest size SMMs currently known. We have also been investigating the derivatization of complex **1** via ligand substitution reactions leading to new forms of the complex with an altered ground-state S value, and this work will be reported in full in due course.[33]

Acknowledgment. We thank the National Science Foundation (CHE-0414555, DMR-0506946 and DMR-0239481) for support of this work.

Supporting Information Available: An X-ray crystallographic file in CIF format for complex **1**·12MeCN, space-filling structural figures, magnetic data, and BVS calculations. This material is available free of charge via the Internet at http://pubs.acs.org.

IC801142P

(33) Stamatatos, Th. C.; Bagai, R.; Abboud, K. A.; Wernsdorfer, W.; Christou, G., in preparation.